Conjugated Polymer Nanoparticles - Graphene Oxide Charge -Transfer Complexes

Emin Istif, Javier Hernández-Ferrer, Esteban Urriolabeitia, Anastasios Stergiou, Nikos Tagmatarchis, Giuseppe Fratta, Matthew J. Large, Alan B. Dalton, Ana M. Benito, Wolfgang K. Maser**

Advanced Functional Materials,
which has been published in final form at DOI: 10.1002/adfm.201707548

This is the **SUBMITTED VERSION** of the following article: Advanced Functional Materials, which has been published in final form at DOI: 10.1002/adfm.201707548

Conjugated Polymer Nanoparticles - Graphene Oxide Charge -Transfer Complexes

Emin Istif, Javier Hernández-Ferrer, Esteban P. Urriolabeitia, Anastasios Stergiou, Nikos Tagmatarchis, Giuseppe Fratta, Matthew J. Large, Alan B. Dalton, Ana M. Benito, Wolfgang K. Maser**

Emin Istif, Dr. Javier Hernández-Ferrer, Dr. Ana M. Benito, Dr. Wolfgang K. Maser
Instituto de Carboquímica (ICB-CSIC), E-50018 Zaragoza, Spain.
Email: wmaser@icb.csic.es, abenito@icb.csic.es; Tel: +34 976 73 39 77

Dr. Esteban P. Urriolabeitia
Instituto de Síntesis Química y Catálisis Homogénea (ISQCH-CSIC Universidad de Zaragoza), E-50009 Zaragoza, Spain

Dr. Anastasios Stergiou, Dr. Nikos Tagmatarchis
Theoretical and Physical Chemistry Institute, National Hellenic Research Foundation, 48 Vassileos Constantinou Avenue, Athens 11635, Greece

Guiseppe Fratta, Dr. Matthew J. Large, Prof. Alan B. Dalton
University of Sussex, Falmer, Brighton BN1, 9RH United Kingdom.

Keywords: conjugated polymers, nanoparticles, graphene oxide, self-assembly, charge-transfer complexes

The game-changing role of GO in tuning the excitonic behavior of conjugated polymer nanoparticles is described for the first time. This is demonstrated by using poly(3-hexylthiophene) (P3HT) as a benchmark conjugated polymer and employing an in-situ re-precipitation approach resulting in P3HT nanoparticles ($P3HT_{NPs}$) with sizes of 50 -100 nm in intimate contact with GO. During the self-assembly process, GO changes the crystalline packing of P3HT chains in the forming $P3HT_{NPs}$ from H to H/J aggregates exhibiting exciton coupling constants as low as 2 meV, indicating favorable charge separation along the P3HT chains. Concomitantly, π-π interface interactions between the $P3HT_{NPs}$ and GO sheets are established resulting in the creation of $P3HT_{NPs}$-GO charge-transfer complexes whose energy bandgaps are lowered by up to 0.5 eV. Moreover, their optoelectronic properties, pre-established in the liquid phase, are retained when processed into thin films from the stable aqueous dispersions, thus eliminating the critical dependency on external processing

parameters. These results can be transferred to other types of conjugated polymers. Combined with the possibility of employing water based "green" processing technologies, charge-transfer complexes of conjugated polymer nanoparticles and GO open new pathways for the fabrication of improved optoelectronic thin film devices.

1. Introduction

Conjugated polymers exhibit outstanding and tunable optoelectronic properties while offering low-cost solution processabiltily.[1] They are widely employed as active layer in organic electronic device structures, such as organic field effect transistors (OFETs), light emitting devices (OLEDs), and solar cells (OSCs).[2] Today they critically contribute to the development of flexible electronic communication platforms and a wide range of ubiquitous electronic commodity products.[3] Their operational functionality strongly depends on efficient charge transport/charge separation characteristics and high carrier mobility. Gaining control on the multifaceted relationship between structure, morphology, interface interactions and optoelectronic properties is key for the successful design of improved conjugated polymer assemblies further boosting device performance.

A benchmark conjugated polymer for this purpose is poly (3-hexylthiophene) (P3HT). Strong intermolecular interactions of the polymer chains afford well-ordered quasi-crystalline domains, i.e. aggregate structures rendering outstanding optoelectronic properties and efficient charge transport pathways through the polymer layer on a macroscopic scale.[4] The influence of chain regularity, polydispersity, and molecular weight on chain order and stacking has been intensively investigated as outlined in the review of K. Tremel.[4] Furthermore, a widely accepted model to discern from spectroscopic observations a specific type of aggregate structure, i.e. H-aggregates for dominant interchain interactions and J-aggregates for dominant intrachain interactions was developed.[5] These studies also emphasize that the formation of well-defined aggregate structures in films of P3HT critically

depends on solvent evaporation effects and crystallization kinetics of the polymer chains during film processing steps. This requires a careful control of the film deposition and post-treatment parameters.

To overcome limitations related to rather extrinsic processing issues, in the last decade, self-assembled P3HT nanostructures with controlled shape and size have attracted increased interest.[6,7] Various studies have shown that the internal aggregate structure, and consequently the optoelectronic properties of resulting nanofibers or nanoparticles can be manipulated by the chain regularity, molecular weight and solvent quality employing mini-emulsion processes.[8–12] Moreover, the aggregate structure, pre-established in the solution, remains preserved when processed into films. This eliminates the dependency on non-intrinsic processing steps and facilitates the fabrication of active layers with defined optoelectronic properties.[9] Furthermore, self-assembly through re-precipitation (or solvent displacement) approaches are of advantage when it comes to the formation of surfactant free aqueous dispersions of P3HT nanoparticles ($P3HT_{NPs}$), thus contributing to film and device fabrication from environmentally-friendly non-toxic dispersions.[13] Recently, this technique also has been successfully used to fabricate core-shell donor-acceptor nanoparticles of $P3HT_{NPs}$ and C_{60} derivative [6,6]-phenyl-C_{61}-butyric acid methyl ester (PCBM) as well as $P3HT_{NPs}$ and CdTe.[14,15]

Here we show that self-assembly processes based on *in-situ* re-precipitation approaches can be effectively employed to create water dispersible $P3HT_{NPs}$-graphene oxide (GO) charge-transfer complexes with tunable optoelectronic properties. GO, a chemically derived sheet of graphene decorated with oxygen containing functional groups on its basal plane and edges, was chosen due to its promise as chemically tunable platform for optoelectronic applications[16,17] and its unique ability to act as an amphiphilic macromolecule.[18] GO thus is ideally suited to self-assemble hierarchical GO structures,[19] such as GO films[20,21] and papers,[22–24] as well as to complex with many organic materials. In combination with

conjugated polymers GO reveals its value as acceptor material[25,26] and provides enhanced conducting and charge-transfer properties.[27,28] GO films also serve as hole-transport and electron transport layer in organic photovoltaic devices.[29] Equally, thin layers of P3HT deposited on GO (and reduced GO) reveal improved charge-transport.[30,31] However, literature describing the interaction of P3HT nanostructures with GO is scarce. A. Chunder investigated the crystallization process of P3HT nanowires on reduced GO,[32] while S. Liu studied the interfacial interactions of P3HT nanofibers deposited on GO films.[33] No work yet has addressed the interactions of GO with $P3HT_{NPs}$ and their effect on the optoelectronic and charge-transport properties.

In this work we explore the interactions established between GO sheets and $P3HT_{NPs}$ during an *in-situ* re-precipitation process carried out in aqueous dispersions containing three different concentrations of GO. The resulting $P3HT_{NP}$-GO hybrid nano-assemblies were investigated in detail by spectroscopic studies (UV-Vis and photoluminescence). They clearly reveal the game-changing role of GO sheets on the internal aggregate structure and excitonic behavior of of $P3HT_{NPs}$. Furthermore, the influence of GO on the charge-transfer properties was probed in thin films by photoluminescence, Raman spectroscopy and electrochemical cyclic voltammetry. These studies demonstrate that the use of GO in liquid phase self-assembly processes facilitates the formation of conjugated polymer nanoparticle-GO charge-transfer complexes with improved and tunable optoelectronic properties, which remain maintained when processed into films from their stable water dispersions. These findings serve as guide for the design of optoelectronic components with superior properties and environmentally friendly processing possibilities.

2. Results and Discussion

The formation of $P3HT_{NPs}$-GO hybrid nano-assemblies was accomplished by an *in-situ* re-precipitation process involving rapid injections of P3HT in THF to excess volume of water dispersions of GO. **Figure 1** illustrates the re-precipitation approach and the resulting stable

This is the **SUBMITTED VERSION** of the following article: Advanced Functional Materials, which has been published in final form at DOI: 10.1002/adfm.201707548

water dispersions containing the $P3HT_{NPs}$ (left-hand route) and $P3HT_{NPs}$-GO nanohybrids (right-hand route) with their respective internal P3HT aggregate structures as revealed by the following microscopy and spectroscopy studies.

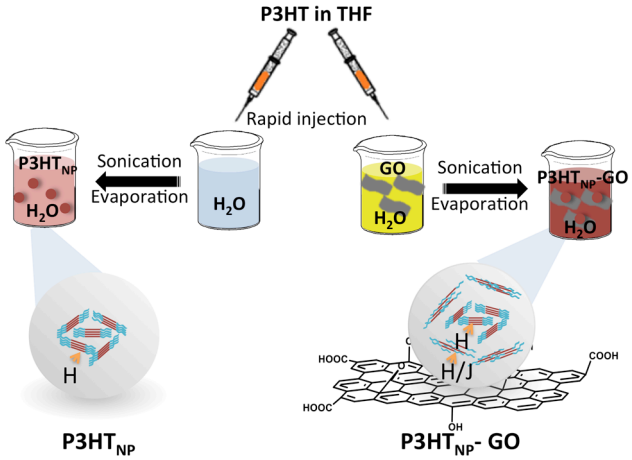

Figure 1. Self-assembly of $P3HT_{NPs}$ and $P3HT_{NPs}$-GO nanohybrids. Aggregated and non-aggregated internal P3HT chains are represented by brown parallel lines and blue wavy lines, respectively. H and H/J indicate the type of aggregate structure.

The morphology of the $P3HT_{NPs}$ polymers and $P3HT_{NPs}$-GO samples was studied by transmission electron microscopy (TEM) and atomic force microscopy (AFM) (**Figure 2**). **Figures 2a, b** reveal that the formation of $P3HT_{NPs}$ was successfully accomplished in the employed re-precipitation method. Particles with sizes in the range of 50 to 200 nm are found (see also statistics in **Figure S4 in S.I.**). **Figures 2c, d** show that $P3HT_{NPs}$ are equally formed in the aqueous GO dispersions.

However, now they always are spotted in close contact with wrinkled sheets of GO, suggesting the creation of intimate interface interactions and thus the formation of true $P3HT_{NPs}$-GO nanohybrids.

This is the **SUBMITTED VERSION** of the following article: Advanced Functional Materials, which has been published in final form at DOI: 10.1002/adfm.201707548

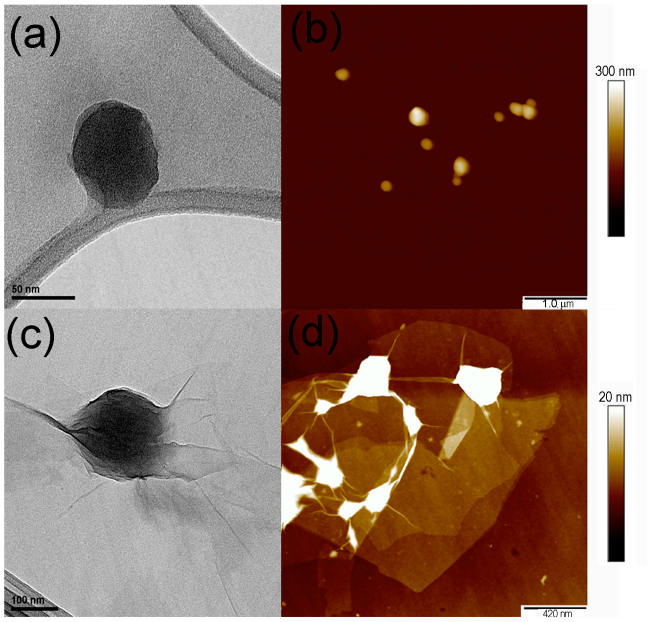

Figure 2. Morphology of $P3HT_{NPs}$ and $P3HT_{NPs}$-GO samples. TEM and AFM images of $P3HT_{NPs}$ (a, b) and $P3HT_{NPs}$-GO (c, d).

To gain insight on the interaction between $P3HT_{NPs}$ and GO, UV-Vis absorption spectroscopy studies were carried out. Spectra of the corresponding hybrid nano-assemblies at different GO concentrations are shown in **Figure 3**. In the range from 350 to 750 nm, $P3HT_{NPs}$ reveal a broad π-π^* transition absorption band exhibiting maxima at 520 nm (2.38 eV). This band can be divided into two parts: A non-structured high-energy region attributed to non-aggregated (disordered) P3HT chains, and a low-energy region characterized by a series of vibronic features indicating the presence of aggregated P3HT chains. These features are typically observed in thin films[4,5] and nanofibers of P3HT.[9,12,34] However, the fact that a similar spectrum already emerges in dispersions is indicative of the morphological change and the formation of $P3HT_{NPs}$ in aqueous media.[8] Due to the insolubility of P3HT in water all P3HT chains are spatially confined within the $P3HT_{NPs}$ and induce aggregation effects discernable through the appearance of vibronic features at the low energy side. Additionally, the formation of crystalline P3HT aggregates is accompanied by a redshift of the absorption maxima of about 400 meV with respect to non-aggregated $P3HT_{THF}$ (see **Figure S5 in S.I.**).

This is the **SUBMITTED VERSION** of the following article: Advanced Functional Materials, which has been published in final form at DOI: 10.1002/adfm.201707548

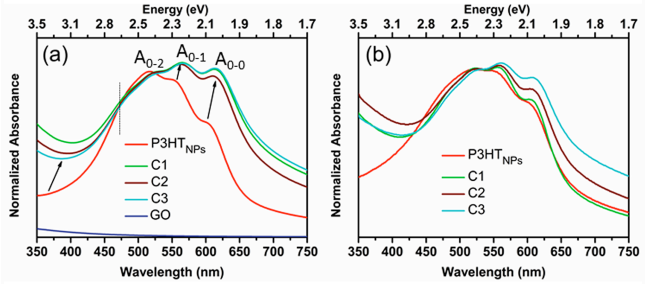

Figure 3. Absorption spectra of P3HTNPs and P3HTNPs-GO samples (labeled Cn, where increasing n denotes decreasing GO concentration) taken from aqueous dispersions (a) and from thin films (b). The spectra are normalized to the intensity of the A0-2 vibronic peak. The featureless spectrum of an aqueous dispersion of GO is included in (a).

For $P3HT_{NPs}$ in aqueous dispersions, three vibronic $A_{0\text{-}n}$ peaks (n refers to the number of vibrational quanta coupled to the electronic transition) are identified at the low-energy side and assigned to $A_{0\text{-}2}$, $A_{0\text{-}1}$, and $A_{0\text{-}0}$ transitions, where $A_{0\text{-}0}$ corresponds to the lowest energy transition. Exploiting the $A_{0\text{-}0}/A_{0\text{-}1}$ intensity ratios provides an easy approach to estimate the interchain excitonic coupling, which is governed largely by intrachain order according to the model introduced by Spano.[35–37] This is based on the observation that the photophysical properties of π-stacked P3HT aggregates depend on the competition between intrachain and interchain coupling. Enhanced interchain interactions favor so-called H-aggregation, i.e. face-to face orientation of the P3HT chains (typically preferred by chains with shorter conjugation lengths or high degree of torsional disorder), while enhanced intrachain interactions favor so-called J-aggregation, i.e end-to-end arrangement of the P3HT chains (facilitated by a high degree of planarity of thiophene rings). By describing a π-stack of a conjugated polymer as an H/J aggregate, the intensity ratio of the $A_{0\text{-}0}$ and the $A_{0\text{-}1}$ vibronic transition is related to the excitonic coupling constant according to

$$\frac{A_{0-0}}{A_{0-1}} = \frac{(1 - 0.96Jo/Ep)^2}{(1 + 0.292Jo/Ep)^2} \quad (1)$$

where J_0 is the coupling constant and E_p is the energy of the coupled phonon mode (taken to be 0.18eV).[5] This model successfully identifies H-type aggregation in thin films and

nanostructures of P3HT.[8-10, 34] $A_{0\text{-}0}/A_{0\text{-}1}$ intensity ratios and J_0 coupling constants for our materials are shown in **Figure 4**. The aqueous dispersions of the parent $P3HT_{NPs}$ reveal an $A_{0\text{-}0}/A_{0\text{-}1}$ ratio of 0.72. Being lower than 1, this value indicates the presence of weakly coupled H-aggregates with a corresponding J_0 coupling constant of +22 meV (**Figure 4a**).

$P3HT_{NPs}$ formed in water in the presence of GO and leading to $P3HT_{NPs}$-GO hybrid nano-assemblies reveal an important enhancement of the $A_{0\text{-}0}/A_{0\text{-}1}$ intensity ratio in the dispersed state approaching values close to 1 and resulting in coupling constants as low as 2 meV (**Figure 4a**). While this still is indicative of weakly coupled H-aggregates it suggests the presence of P3HT chains with low disorder and high planarity confined in the $P3HT_{NPs}$. This further is supported by a redshift of the vibronic peaks by about 30 meV (**Figure 4b**). Already achieved at the lowest amount of GO, it appears that GO induces the formation of highly planar P3HT chains in the $P3HT_{NPs}$. It thus plays the role of a "good" solvent additive for the conjugated polymer during the formation of $P3HT_{NPs}$, in analogy to the work of Barnes and Venkataraman, who pointed out that the use of "marginal" and "good" solvent mixtures in the self-assembly process improve the aggregate structure in pure $P3HT_{NPs}$.[8] The change of the solvent quality in the re-precipitation process also can be understood as a consequence of the amphiphilic character of the GO sheets, as described by Huang and co-workers.[18] Being homogeneously dispersed in the water phase, in close vicinity to the forming $P3HT_{NPs}$ they can act as two- dimensional surfactant templates and induce a higher planarity of the internal P3HT chains. This lowers the surface tension at the interface of the $P3HT_{NPs}$ and the GO sheets and contributes to stabilize the $P3HT_{NPs}$-GO hybrid structure. The observation that an already formed aggregation structure of $P3HT_{NPs}$ cannot be modified upon subsequent mixing with a water dispersion of GO (UV-Vis spectra for the ex-situ mixing process are shown in **Figure S6** (see S.I.) further underlines the solvent effect of GO and its immediate impact on the aggregation structure during the rapid liquid phase re-precipitation process.

This is the **SUBMITTED VERSION** of the following article: Advanced Functional Materials, which has been published in final form at DOI: 10.1002/adfm.201707548

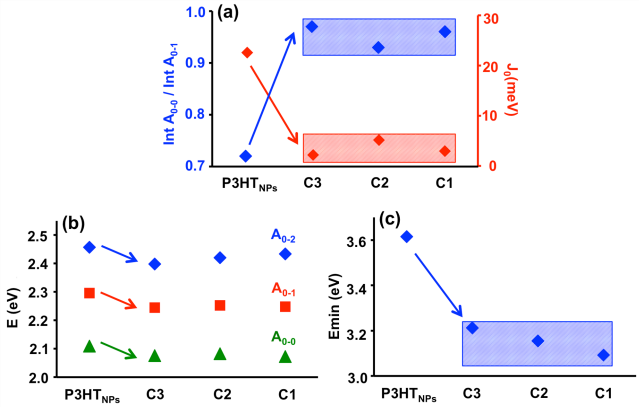

Figure 4. Values derived from the UV-Vis absorption spectra of aqueous dispersions of P3HT$_{NPs}$ and P3HT$_{NPs}$-GO samples (labeled Cn, n = 3, 2, 1, from lowest to highest GO concentration, respectively). (a) Intensity ratio of the vibronic A_{0-0} to A_{0-1} transitions (blue) and excitonic coupling constant J_0 (red), (b) Energy position of the A_{0-2}, A_{0-1}, A_{0-0} vibronic transitions, and (c) Energy position of the minima at the high-energy side of π-π* band.

Looking at the non-structured high-energy side of the absorption spectrum, which is attributed to disordered P3HT chains in the P3HT$_{NPs}$, a redshift of the minima by about 0.4 to 0.5 eV is encountered for the P3HT$_{NPs}$-GO samples (**Figure 4c**). While mostly pronounced at lowest GO concentrations, the redshift further progresses by several tens of meV with enhanced GO concentration. This suggests the existence of favorable interface interactions between the GO sheets and the less ordered P3HT chains at the periphery of the P3HT$_{NPs}$. Consequently, the interacting P3HT chains within the P3HT$_{NPs}$ adopt a higher degree of planarity and contribute to the formation of H-aggregates with reduced interchain coupling, i.e. H/J aggregates, in agreement with the intensity changes of the vibronic peaks observed at the low-energy side of the spectra. While P3HT$_{NPs}$-GO interface interaction effects are expressed at the high-energy side of the spectra, they go along with changes of the low-energy vibronic transitions. It thus becomes clear that enhanced P3HT intrachain order and reduced interchain coupling of the P3HT aggregates are intimately linked to each other as a result of the interaction of P3HT$_{NPs}$ with GO sheets established during the *in-situ* self-assembly process in the aqueous dispersion. The existence of an isobestic point (**Figure 3a**) at about 475 nm (2.61 eV) nicely illustrates the convergence of both effects.

For thin films of $P3HT_{NPs}$ and $P3HT_{NPs}$-GO the spectra essentially maintain the features acquired in the dispersion state (**Figure 3b**). This refers to the presence of the vibronic structure, the enhancement of the A_{0-0} to A_{0-1} intensity ratio and the redshift of the high-energy minima in the nanohybrids (see **Figure S8 in S.I.**). While the respective values may somewhat differ from the case of dispersions, nanomorphology and aggregate structure remain preserved. Solvent evaporation effects during film formation seem to play a negligible role in case of the nanohybrids, which is of importance for the fabrication of thin film devices based on $P3HT_{NPs}$-GO nanohybrids with a well-defined nanomorphology and aggregation structure pre-established in the dispersion state.

Valuable complementary information on aggregation and interaction effects is obtained from photoluminescence studies (**Figure 5**). The spectra of $P3HT_{NPs}$ and the $P3HT_{NPs}$-GO series exhibit a broad emission ranging from 600 to 800 nm. This is composed of two well defined (yet still quite broad) vibronic bands located at about 650 nm (1.90 eV) and 710 nm (1.75 eV) with an intensity ratio of about 1.35, accompanied by a not well defined third band at about 800 nm (1.55 eV) of very low intensity. This landscape resembles the one encountered for P3HT films where H-aggregates are the only emitting species.[4, 5, 9, 10] In agreement with the results from absorption spectroscopy, this clearly confirms the presence of H-aggregates in $P3HT_{NPs}$, which are identified as the sole origin for the observed photoluminesce spectra. On the other hand, the H- character of the spectra inherently involves the existence of disordered P3HT chains in the $P3HT_{NP}$, which defines the broadness of the vibronic transitions.[4, 5, 10] Moreover, identical spectral features of $P3HT_{NPs}$ in the form of thin films (Figure 5b) reveals that the H-character of the aggregates is kept unaltered in the solid state.

The spectra of the $P3HT_{NPs}$-GO samples essentially show the same features as the bare $P3HT_{NPs}$, with negligible changes in the positions of the vibronic peaks. However, in dispersion a significant increase of the emission intensity of up to 50 % with respect to the corresponding $P3HT_{NPs}$ is observed (**Figure 5a, c**).

This is the **SUBMITTED VERSION** of the following article: Advanced Functional Materials, which has been published in final form at DOI: 10.1002/adfm.201707548

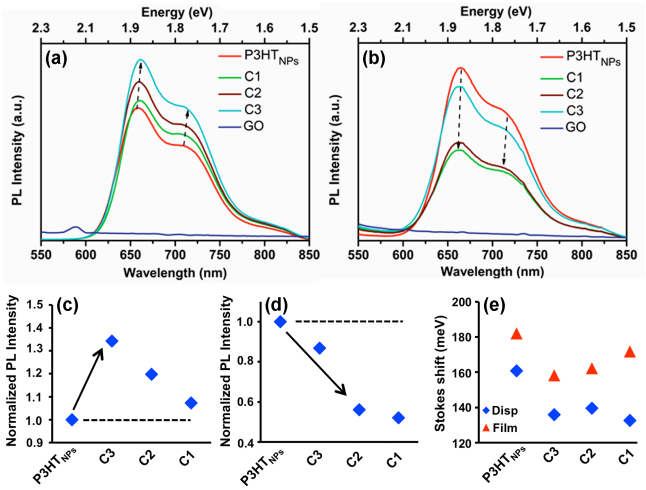

Figure 5. Photoluminescence emission spectra (λ_{exc} = 490 nm) of GO, P3HT$_{NPs}$ and P3HT$_{NPs}$-GO samples (labeled Cn, n=3, 2, 1, from lowest to highest GO concentration, respectively) for aqueous dispersions (a) and thin films (b). Normalized integrated photoluminescence intensities for dispersions (c) and thin films (d). Stokes shifts (e) as determined from the energy differences of the position of the high energy photoluminescence band maximum and the position of the low energy $A_{0\text{-}0}$ vibronic transition.

While this looks surprising at first sight, it rather reflects the results obtained from absorption spectroscopy. Here an important enhancement of H-aggregates (i.e. H-aggregates with reduced interchain coupling, also called H/J aggregates) is seen already for the lowest GO concentration. Being only sensitive to the internal H-aggregate structure, the enhancement in PL intensity reflects the existence of an higher amount of H-aggregates in the spherical P3HT$_{NPs}$ due to the fact that GO in the synthesis process acts as a "good" solvent additive, as described above. At the lowest concentrations it facilitates the enhanced formation of H-aggregates, which, towards the periphery of the nanoparticles, adopt a more H/J-like character. Thus, a larger overall volume of H-aggregates is available in the NPs contributing to the enhancement of the photoluminescence. At higher GO concentrations the emission intensity is reduced, but still remaining higher compared to the bare P3HT$_{NPs}$. The lowering in intensity is explained by a decreased GO solvent effect, i.e. a less effective formation of H-aggregates and/or by a reduced dispersibility upon the increase of GO in the aqueous dispersion.

A completely different situation is observed for the case of thin films where significant quenching by up to 50 % is observed with increased amounts of GO (**Figure 5b, d**). While in dispersion the photoluminescence is governed by the enhanced H-character of the $P3HT_{NPs}$ due to the performance of GO as a "good" solvent, in films, as a result of the (non-isotropic) deposition process, the emission behavior is dominated by the intimate contact between GO sheets and P3HT chains at the surface of the $P3HT_{NPs}$. The interface established between GO and $P3HT_{NPs}$, characterized by P3HT chains of a higher planarity owing to favorable π-π interface interactions, thus results in the formation of a charge-transfer complex which effectively facilitates the charge separation process in the solid state. Enhanced possibilities for intimate interface interactions contributing to improved charge separation processes are established, up to a certain limit, for $P3HT_{NPs}$-GO films fabricated from dispersions containing higher GO contents (**Figure 5d**).

Finally, a reduction in the Stokes-shift (**Figure 5e**) by about 25 meV when comparing bare $P3HT_{NPs}$ with $P3HT_{NPs}$-GO nanohybrids (for dispersion and films) is in agreement with the observed 30 meV redshift of the vibronic peaks in the absorption spectra. This corroborates the existence of enhanced amounts of H-aggregates with reduced interchain coupling (indicative for the presence of P3HT chains with lower torsional defects and improved coherence length) towards the periphery of the P3HT nanoparticles. Changes of the internal aggregate structure of $P3HT_{NPs}$ upon interaction with GO are depicted in Figure 1.

To further investigate the interaction between $P3HT_{NPs}$ and GO, Raman measurements were carried out on films of $P3HT_{NPs}$, $P3HT_{NPs}$-GO and GO using an excitation wavelength of 785 nm (**Figure 6**). In the range from 1000 to 1750 cm^{-1}, $P3HT_{NPs}$ exhibit two dominant sharp peaks at around 1445 cm^{-1} and 1380 cm^{-1}, assigned to the symmetric C=C (C_α=C_β) and C–C (C_β–C_β) ring stretch modes of the thiophene ring, respectively[38]. GO shows two broad bands at 1598 cm^{-1} and 1318 cm^{-1}, corresponding to the G-band (tangential C-C stretch modes of

graphene sheets) and the D-band (related to defects, i.e. the presence of sp^3 hybridized carbon in the oxidized graphene sheets), respectively.[39]

The spectra of the $P3HT_{NPs}$-GO samples are characterized by the broad G and D band of GO and the superposition of the two sharp ring-stretch modes of $P3HT_{NPs}$. The GO related bands are clearly visible in the $P3HT_{NPs}$-GO nanohybrids already at the lowest GO concentration. Even more important, there is a significant softening of both the G and the D line by up to 10 cm-1 observable already for the lowest content of GO (**Figure 6b**). Such softening typically is associated with electron injection from P3HT chains to graphene-based nanostructures, as observed for reduced graphene oxide[40] or carbon nanotubes.[41] These results further support that charge-transfer is taking place at the interface between P3HT and GO, acting as electron donor and acceptor, respectively. Furthermore, the intensity ratio of the C=C to C–C ring stretch modes (Figure 6c), analyzed from background subtracted spectra, reveals a clear decrease with increasing GO concentration. This is consistent with an enhanced quinoid character, as consequence of an effective charge-transfer.

This is the **SUBMITTED VERSION** of the following article: Advanced Functional Materials, which has been published in final form at DOI: 10.1002/adfm.201707548

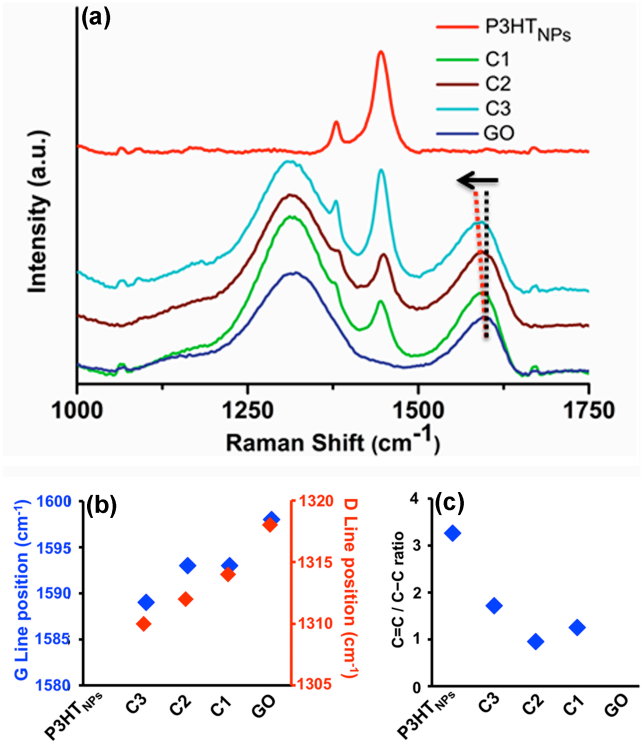

Figure 6. (a) Raman spectra (λ_{exc} = 785 nm) of films of P3HT$_{NPs}$ and P3HT$_{NPs}$-GO composites (labeled Cn, n=3, 2, 1, from lowest to highest GO concentration, respectively), (b) Position of G and D line, (c) Intensity ratio of P3HT C=C/C–C ring stretch mode.

Finally, cyclic voltammetry (CV) studies further provided valuable complementary information on issues of aggregation, charge-transfer, and HOMO and LUMO energy levels. **Figure 7** shows the CV curves of the P3HT$_{NPs}$, and P3HT$_{NPs}$-GO samples obtained after applying 10 continuous pre-cycles in the range of -1.5 to 1.2 V (details on the pre-cycling studies can be found in **Figure S9 of S.I.**).

This is the **SUBMITTED VERSION** of the following article: Advanced Functional Materials, which has been published in final form at DOI: 10.1002/adfm.201707548

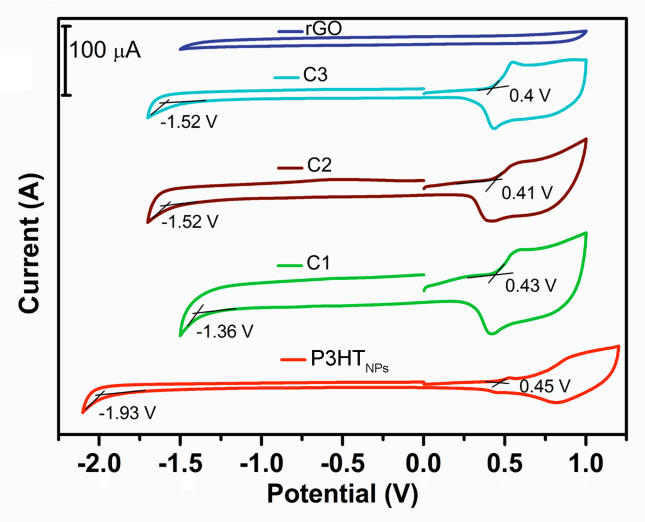

Figure 7. Cyclic voltammograms of films of $P3HT_{NPs}$ and $P3HT_{NPs}$-GO samples (labeled Cn, n=3, 2, 1 from lowest to highest GO concentration, respectively). Potential values are given with respect to Ag/AgCl used as reference electrode. Values of on-set oxidation and reduction positions are indicated. The curve for electrochemically reduced GO is shown for comparison. Scan rates of 100 mV/s were employed.

The CV response of $P3HT_{NPs}$ is characterized by two oxidation peaks located at about 0.55 and 0.85 V. The lower one is attributed to the presence of aggregated P3HT chains and the higher one to amorphous or a mixture of amorphous and aggregated P3HT chains.[42] The onset-value of the oxidation and reduction peaks (indicated in Figure 8), determined as the crossing point of the slopes of the peaks with the background current, are used to calculate the HOMO and LUMO energy levels of P3HT and the corresponding energy gap (**Table 1**).

This is the **SUBMITTED VERSION** of the following article: Advanced Functional Materials, which has been published in final form at DOI: 10.1002/adfm.201707548

Table 1. Energy values for HOMO and LUMO levels and derived energy bandgaps, determined from the on-set values of the oxidation and the reduction peaks, for $P3HT_{NPs}$ and $P3HT_{NPs}$-GO samples (labelled Cn, n=3, 2, 1 from lowest to highest GO concentration, respectively).

Sample	E_{HOMO} (eV)*	E_{LUMO} (eV)*	E_{gap}(eV)*
$P3HT_{NPs}$	-5.05	-2.67	2.38
C3	-5.00	-3.08	1.92
C2	-5.01	-3.08	1.93
C1	-5.03	-3.24	1.79

*E_{HOMO} =-[E_{onset} (ox) + 4.6] (eV); E_{LUMO} = -[E_{onset} (red) + 4.6] (eV);[43] E_{gap} = E_{LUMO}-E_{HOMO}

For the $P3HT_{NPs}$-GO samples a significant enhancement of the low oxidation peak with respect to the high oxidation peak indicates a significant increase of aggregated P3HT chains. This can be clearly seen already for the lowest concentration of GO. An accompanying downshift of the oxidation on-set potential (HOMO level) by about 50 meV further underlines the enhancement of aggregated P3HT domains with respect to the original $P3HT_{NPs}$. This situation fully coincides with the observation in absorption spectroscopy where intensity changes and redshifts of the vibronic modes by several tens of meV confirm the presence of enhanced amounts of H/J aggregates in the $P3HT_{NPs}$ of the $P3HT_{NPs}$-GO nanohybrids.

Looking at the reduction on-set potentials (LUMO levels) considerable shifts of 400 to 500 meV towards more positive potentials for the lowest GO concentration are observed, progressing by several tens of meV for higher GO concentrations. This fully coincides with the redshifts of the minima in the low-energy shoulder in absorption spectroscopy, which are attributed to the π-π interface interactions of GO sheets with the disordered P3HT chains located at the surface of the $P3HT_{NPs}$. Effective interface interactions (discernable by lower absolute values of the on-set reduction potential), which are the origin of charge-transfer processes as witnessed by photoluminescence and Raman spectroscopy, coupled to the enhancement of H/J domains (notable by lower absolute values of the on-set oxidation potential), lead to an important decrease of the HOMO-LUMO energy gap in $P3HT_{NPs}$-GO

nanohybrids with respect to the original $P3HT_{NPs}$. This further is accompanied by an enhancement of the overall current response with increasing GO concentration. These observations consistently suggest the formation of stabilized $P3HT_{NPs}$-GO charge-transfer complexes with reduced excitonic coupling, achieved during the synthesis in the liquid state and maintained in the solid state. The $P3HT_{NPs}$-GO nanohybrid charge-transfer complexes with their liquid-phase predefined properties thus may serve as model systems providing unique opportunities for the development of improved optoelectronic thin film devices based on charge-transfer complexes of conjugated polymer nanoparticles and GO.

3. Conclusions

In this work we show for the first time the game-changing role of GO in tuning the excitonic behaviour of conjugated polymer nanoparticles and the efficient formation of conjugated polymer nanoparticle-GO charge-transfer complexes. We demonstrate this by using P3HT as a benchmark conjugated polymer and applying a novel in-situ re-precipitation approach, in which P3HT assembles into nanoparticles ($P3HT_{NPs}$) with sizes of 50 – 200 nm being in intimate contact with surrounding GO sheets. We prove that during the self-assembly process GO plays the role of a "good" solvent additive in the marginal water phase resulting in a significant enhancement of the planarity of the P3HT chains in the forming $P3HT_{NPs}$. This creates a two-fold win-win situation: (a) Change of the crystalline packing of the internal P3HT chains from an original H-type towards an H/J aggregate structure with excitonic coupling constants as low as 2 meV, favoring charge separation along the P3HT chains. (b) Establishment of effective π-π interface interactions between the $P3HT_{NPs}$ and the GO sheets. This enables the formation of stable $P3HT_{NPs}$-GO charge-transfer complexes whose energy bandgaps, as a function of GO content, are lowered by up to 0.5 eV, with respect to $P3HT_{NPs}$. Moreover, the morphology, aggregate structure and optoelectronic properties pre-established in the liquid phase are maintained when processed into thin films from their stable aqueous

$P3HT_{NPs}$-GO dispersions, thus eliminating the critical dependency of the operational functionality of devices on rather extrinsic processing parameters. The results are of general character and can be transferred to other types of conjugated polymers. Controlling the optoelectronic properties of conjugated polymer nanoparticles by GO in the liquid phase and preserving them in the form of thin films, combined with the possibility to employ "green" processing technologies, opens new pathways for the design of improved optoelectronic thin film devices.

4. Experimental Section

4.1. Materials

3-hexyl thiophene, [1,3-Bis(diphenylphosphino)propane] dichloronickel(II)] ($Ni(dppp)Cl_2$), tert-BuMgCl (1M THF solution), dry DMF, THF, N-Bromosuccinimide, acetonitrile, HCl were purchased from Sigma-Aldrich and were used as received. THF was distilled over benzophenone and sodium. $NaClO_4$ was dried overnight at 130^0C in vacuum oven before use. Graphene oxide in aqueous dispersion (4mg/mL) was acquired from Graphenea S.L. (San Sebastian, Spain).

4.2. Synthesis of $P3HT_{NPs}$-GO

First, P3HT with a regioregularity of 92 %, a molecular weight of 8100 and a polydispersity index of 1.19 was synthesized using a Grignard metathesis polymerization process. Synthesis details, ^{1}H-NMR spectra, characterization of polymer regioregularity and molecular weights are detailed in Supporting Information. The synthesized P3HT was added to THF in a concentration of 1mg/mL and left to dissolve under magnetic stirring overnight at room temperature. The polymer solution (2 mL) was injected into an aqueous solution of GO under vigorous stirring (2 mg in 10 mL, 1 mg in 10 mL and 0.5 mg in 10 mL). In order to increase the dispersibility a tip sonicator was used for 3 min. Remaining THF was evaporated *via* a vacuum evaporator operating at 35 ºC. Lastly, dispersions were filtered and supernatant used

for further experiments. The samples were obtained using the following P3HT : GO weight ratios: 1 : 0 ($P3HT_{NPs}$); 1 : 0.25 (C3); 1 : 0.5 (C2), and 1 : 1 (C1). Sample denomination is given in parenthesis.

4.3. Characterization

^{1}H-NMR spectra were recorded in $CDCl_3$ solutions at 25 ºC on a Bruker AV500 spectrometer (δ in ppm and J in Hz) at a ^{1}H NMR operating frequency of 500.13 MHz. UV/Vis absorption spectra from dispersions and from films spray coated on cleaned glass substrates were recorded on a Shimadzu UV-2401 PC spectrophotometer. The concentrations of the dispersions and film thicknesses were carefully adjusted to obtain comparable optical densities for the π-π* absorption band for each of the series of dispersions and films. Photoluminescence emission spectra were recorded on a Horiba Jobin Yvon Fluoromax-P, from dispersions used in UV-Vis spectroscopy using a 10 mm path-length quartz cuvette and from films spray coated on cleaned silicon oxide substrates. Raman spectroscopy was performed on the films coated on silicon oxide substrates using a Horiba Jobin-Yvon HRLAB HR 800 UV apparatus (λ_{exc}= 785 nm). TEM images were acquired in a JEOL microscope model 2000 FXII at an acceleration potential of 200 kV. Aqueous dispersions were drop-cast on lacey carbon TEM grids followed by a room temperature drying process to evaporate the aqueous solvent.

AFM images on films drop-casted on Si/SiO_2 substrates (previously cleaned with isopropanol and treated with ozone cleaner for 10 min) were obtained with a Bruker Dimension Icon®, in Scanasyst® mode using a PFQNE-AL ® tip with a 5 nm diameter. Images were taken with a 512 sampling/line resolution at a frequency of 1 Hz. Scanasyst mode is a proprietary PeakForce Tapping ® mode developed by Bruker that employs automatic optimization algorithms to actively check image quality and consequently chooses the most appropriate amplitude, frequency and amplitude set-point values.

Molecular weight distributions of the samples were determined by size exclusion chromatography (SEC) using a Waters system, composed of a Waters 1515 isocratic pump, a set of three μ-Styragel mixed bed columns (having a porosity range of 10^2 to 10^6 Å), a Waters 2414 refractive index detector (equilibrated at 40 ºC) and controlled through Breeze software. Tetrahydrofuran was the mobile phase, used at a flow rate of 1.0 mL/min at 30 ºC. The setup was calibrated with linear polystyrene standards having narrow polydispersity and average molecular weights in the range of 1200 to 929,000 g/mol. The samples were readily soluble in the mobile phase. Concentrations in the range 2-4 mg/mL were used for analysis.

The electrochemical experiments were performed with a AUTOLAB PGSTAT302N potentiostat. Cyclic voltammetry (CV) of composites were carried out under nitrogen in a three- electrode cell using 0.1 M $NaClO_4$ in dry acetonitrile as a supporting electrolyte. Scan rates of 100 mV/s were employed. Glassy carbon, platinum plate and silver/silver chloride were used as working electrode, counter electrode and reference electrode, respectively. The samples were drop-casted on the glassy carbon electrode. For composites and GO films 10 continuous pre-cycles in the range of -1.5 to 1.2 V were applied to obtain stable CV responses.

Supporting Information

Supporting Information is available from the Wiley Online Library or from the author.

Acknowledgements

This work has received funding from the European Union's Horizon 2020 research and innovation programme under the Marie Skłodowska-Curie grant agreement No 642742. AMB, and WKM acknowledge Spanish MINEICO (project ENE2016-79282-C5-1-R and associated EU Regional Development Funds), and the Gobierno de Aragón (Consolidated Group DGA-T66-GCNN and associated EU Social Funds).

This is the **SUBMITTED VERSION** of the following article: Advanced Functional Materials, which has been published in final form at DOI: 10.1002/adfm.201707548

Received: ((will be filled in by the editorial staff))
Revised: ((will be filled in by the editorial staff))
Published online: ((will be filled in by the editorial staff))

References

[1] H. Shirakawa, J. Louis, A. G. Macdiarmid, *J. C. S. Chem. Comm.* **1977**, 16, 578.

[2] T. A. Skotheim and J. R. Reynolds, eds., *Handbook of Conducting Polymers*; CRC Press: Boca Raton, FL, 2007.

[3] W. Park, ed., *Chem. Soc. Rev.* **2010**, 39, *2337-2732*.

[4] K. Tremel, S. Ludwigs, *Adv. Polym. Sci.*; **2014**, 265, 39–82.

[5] F. C. Spano, C. Silva, *Annu. Rev. Phys. Chem.* **2014**, *65*, 477.

[6] D. Tuncel, H. V. Demir, *Nanoscale* **2010**, *2*, 484.

[7] J. Pecher, S. Mecking, *Chem. Rev.* **2010**, *110*, 6260.

[8] G. Nagarjuna, M. Baghgar, J. A. Labastide, D. D. Algaier, M. D. Barnes, D. Venkataraman, *ACS Nano* **2012**, *6*, 10750.

[9] M. Baghgar, M. D. Barnes, *ACS Nano* **2015**, *9*, 7105.

[10] E. T. Niles, J. D. Roehling, H. Yamagata, A. J. Wise, F. C. Spano, A. J. Moulé, J. K. Grey, *J. Phys. Chem. Lett.* **2012**, *3*, 259.

[11] J. Gao, B. W. Stein, A. K. Thomas, J. A. Garcia, J. Yang, M. L. Kirk, J. K. Grey, *J. Phys. Chem. C* **2015**, *119*, 16396.

[12] J. D. Roehling, I. Arslan, A. J. Moulé, *J. Mater. Chem.* **2012**, *22*, 2498.

[13] H. Shimizu, M. Yamada, R. Wada, M. Okabe, *Polym. J.* **2008**, *40*, 33.

[14] S. Chambon, C. Schatz, V. Sébire, B. Pavageau, G. Wantz, L. Hirsch, *Mater. Horiz.* **2014**, *1*, 431.

[15] E. Istif, A. Kagkoura, J. Hernández-Ferrer, A. Stergiou, T. Skaltsas, R. Arenal, A.M. Benito, W.K. Maser, N. Tagmatarchis, *ACS Appl. Mater. Interfaces* **2017**, DOI: 10.1021/acsami.7b13506.

[16] K. P. Loh, Q. Bao, G. Eda, M. Chhowalla, *Nat. Chem.* **2010**, *2*, 1015.

[17] G. Eda, M. Chhowalla, *Adv. Mater.* **2010**, *22*, 2392.

[18] J. Kim, L. J. Cote, F. Kim, W. Yuan, K. R. Shull, J. Huang, *J. Am. Chem. Soc.* **2010**, *132*, 8180.

[19] Y. Xu, G. Shi, *J. Mater. Chem.* **2011**, *21*, 3311.

[20] L. J. Cote, F. Kim, J. Huang, *J. Am. Chem. Soc.* **2009**, *131*, 1043.

[21] G. Eda, G. Fanchini, M. Chhowalla, *Nat. Nanotechnol.* **2008**, *3*, 270.

[22] D. A. Dikin, S. Stankovich, E. J. Zimney, R. D. Piner, G. H. B. Dommett, G. Evmenenko, S. T. Nguyen, R. S. Ruoff, *Nature* **2007**, *448*, 457.

[23] C. Vallés, J. David Núñez, A. M. Benito, W. K. Maser, *Carbon N. Y.* **2012**, *50*, 835.

[24] J. D. Núñez, A. M. Benito, S. Rouzière, P. Launois, R. Arenal, P. M. Ajayan, W. K. Maser, *Chem. Sci.* **2017**, *8*, 4987.

[25] C. Vallés, P. Jiménez, E. Muñoz, A. M. Benito, W. K. Maser, *J. Phys. Chem. C* **2011**, *115*, 10468.

[26] M. M. Stylianakis, E. Stratakis, E. Koudoumas, E. Kymakis, S. H. Anastasiadis, *ACS Appl. Mater. Interfaces* **2012**, *4*, 4864.

[27] R. Bkakri, N. Chehata, A. Ltaief, O. E. Kusmartseva, F. V. Kusmartsev, M. Song, A. Bouazizi, *J. Phys. Chem. Solids* **2015**, *85*, 206.

[28] Q. Liu, Z. Liu, X. Zhang, L. Yang, N. Zhang, G. Pan, S. Yin, Y. Chen, J. Wei, *Adv. Funct. Mater.* **2009**, *19*, 894.

[29] J. Liu, M. Durstock, L. Dai, *Energy Environ. Sci.* **2014**, *7*, 1297.

[30] A. Liscio, G. P. Veronese, E. Treossi, F. Suriano, F. Rossella, V. Bellani, R. Rizzoli, P. Samorì, V. Palermo, *J. Mater. Chem.* **2011**, *21*, 2924.

[31] S. Wang, C. T. Nai, X.-F. Jiang, Y. Pan, C.-H. Tan, M. Nesladek, Q.-H. Xu, K. P. Loh, *J. Phys. Chem. Lett.* **2012**, *3*, 2332.

[32] A. Chunder, J. Liu, L. Zhai, *Macromol. Rapid Commun.* **2010**, *31*, 380.

[33] S. Liu, X. Ma, B. Wang, X. Shang, W. Wang, X. Yu, *Macromolecules* **2015**, *48*, 5791.

[34] Y. Yuan, J. Shu, P. Liu, Y. Zhang, Y. Duan, J. Zhang, *J. Phys. Chem. B* **2015**, *119*, 8446.

[35] F. C. Spano, *J. Chem. Phys.* **2005**, *122*, 234701.

[36] J. Clark, C. Silva, R. H. Friend, F. C. Spano, *Phys. Rev. Lett.* **2007**, *98*, 206406.

[37] J. Clark, J.-F. Chang, F. C. Spano, R. H. Friend, C. Silva, *Appl. Phys. Lett.* **2009**, *94*, 163306.

[38] W. C. Tsoi, D. T. James, J. S. Kim, P. G. Nicholson, C. E. Murphy, D. D. C. Bradley, J. Nelson, J.-S. Kim, *J. Am. Chem. Soc.* **2011**, *133*, 9834.

[39] A. C. Ferrari, J. Robertson, *Phys. Rev. B* **2000**, *61*, 14095.

[40] Q. Su, S. Pang, V. Alijani, C. Li, X. Feng, K. Müllen, *Adv. Mater.* **2009**, *21*, 3191.

[41] A. Bakour, F. Geschier, M. Baitoul, J. Wéry, F. Massuyeau, E. Faulques, *Mater. Chem. Phys.* **2016**, *171*, 83.

[42] S. Sweetnam, K. R. Graham, G. O. Ngongang Ndjawa, T. Heumüller, J. A. Bartelt, T. M. Burke, W. Li, W. You, A. Amassian, M. D. McGehee, *J. Am. Chem. Soc.* **2014**, *136*, 14078.

[43] S. Trasatti, *Pure Appl. Chem.* **1986**, *58,* 955.

This is the **SUBMITTED VERSION** of the following article: Advanced Functional Materials, which has been published in final form at DOI: 10.1002/adfm.201707548

Table of contents entry

Nanoparticles of conjugated polymer P3HT self-assembled in the presence of graphene oxide (GO) reveal an internal aggregate structure with significantly reduced excitonic coupling constants, which concomitantly favors π-π interactions with graphene oxide sheets towards the formation of a charge-transfer complexes with reduced energy bandgaps.

Keywords: conjugated polymers, nanoparticles, graphene oxide, self-assembly, charge-transfer complexes

Emin Istif, Javier Hernández-Ferrer, Esteban Urriolabeitia, Anastasios Stergiou, Nikos Tagmatarchis, Giuseppe Fratta, Matthew J. Large, Alan B. Dalton, Ana M. Benito, Wolfgang K. Maser**

Conjugated Polymer Nanoparticles - Graphene Oxide Charge - Transfer Complexes

ToC figure